Lab on a Chip

Computer Vision Enabled Funnel Adapted Sensing Tube (FAST) for Power-Free and Pipette-Free Nucleic Acid Detection

Journal:	*Lab on a Chip*
Manuscript ID	LC-ART-06-2022-000586.R1
Article Type:	Paper
Date Submitted by the Author:	16-Aug-2022
Complete List of Authors:	Bao, Mengdi; Rochester Institute of Technology, Zhang, Shuhuan; Rochester Institute of Technology ten Pas, Chad; Rochester Institute of Technology Dollery, Stephen; Biological Mimetics Inc Bushnell, Ruth; Biological Mimetics Inc Yuqing, FNU; Rochester Institute of Technology Liu, Rui; Rochester Institute of Technology Lu, Guoyu; University of Georgia Tobin, Gregory; Biological Mimetics Inc Du, Ke; Rochester Institute of Technology

ARTICLE

Computer Vision Enabled Funnel Adapted Sensing Tube (FAST) for Power-Free and Pipette-Free Nucleic Acid Detection

Received 00th January 20xx,
Accepted 00th January 20xx

DOI: 10.1039/x0xx00000x

Mengdi Bao,[a] Shuhuan Zhang,[a] Chad ten Pas,[a] Stephen J. Dollery,[b] Ruth V. Bushnell,[b] FNU Yuqing,[a] Rui Liu,[a] Guoyu Lu,[c] Gregory J. Tobin,[b] and Ke Du [a] *

A simple, portable, and low-cost microfluidic chip-Funnel Adapted Sensing Tube (FAST) is developed as an integrated, power-free, and pipette-free biosensor for viral nucleic acids. This FAST chip consists of four reaction chambers separated by carbon fiber rods, and the reagents in each chamber are transferred and mixed by manually removing the rods. Rather than using electrical heaters, only a hand warmer pouch is used for an isothermal recombinase polymerase amplification and CRISPR-Cas12a reaction. The signal produced by the RPA-CRISPR reaction is observed by the naked eye using an inexpensive flashlight as a light source. The FAST chip is fabricated using water-soluble polyvinyl alcohol (PVA) as a sacrificial core, which is simple and environmentally friendly. Using a SARS-CoV-2 fragment as a target, a ~10 fM (6 x 10^3 copies/µL) detection limit is achieved. To generalize standard optical readout for individuals without training, a Linear Kernel algorithm is created, showing an accuracy of ~100% for identifying both positive and negative samples in FAST. This power-free, pipette-free, disposable, and simple device will be a promising tool for nucleic acid diagnostics in either clinics or low-resource settings.

Introduction

The coronavirus disease 2019 (COVID-19) pandemic caused by severe acute respiratory syndrome coronavirus 2 (SARS-CoV-2) has spread across the globe and has become a significant threat to human life. According to the World Health Organization, the pandemic has resulted in over 550 million confirmed cases, and 6 million deaths as of August 2022.[1] This highlights the need for rapidly adaptable technology for the early and sensitive detection of newly emerging and existing diseases.[2,3] Recently, various nucleic acid, protein, and antibody-based diagnostics have been developed, but all have their limitations. Today, real-time reverse transcription polymerase chain reaction (RT-PCR) still remains the gold standard.[4,5] Even though highly sensitive and specific, RT-PCR requires well-trained personnel and electrical instruments, thus limiting its utility in resource-constrained settings.[6,7]

Clustered regularly interspaced short palindromic repeats (CRISPR)-associated (Cas) proteins emerged as a promising tool for nucleic acid detection.[8,9] Some Cas nucleases, particularly Cas12a and Cas13, can cleave non-targeted single-stranded nucleic acids once they have identified targets.[10,11] This unique property has demonstrated high sensitivity in nucleic acid detection by non-specifically cleaving fluorophore-quencher probes. Upon recognition of targets, the activated Cas nucleases degrade fluorophore-quencher nucleic acids, thereby generating an increase in fluorescence signal. The CRISPR-Cas detection also exhibits high specificity and can be performed isothermally, making it an excellent alternative to RT-PCR detection.[12,13] To further improve sensitivity and enable sensitive diagnostics, CRISPR assays have been combined with isothermal amplification, such as recombinase polymerase amplification (RPA), rolling circle amplification (RCA), and loop-mediated isothermal amplification (LAMP).[14,15,16] Among these, RPA is a widely used amplification method as it is simple, rapid, and can be performed at the same temperature as CRISPR assays. However, most RPA-CRISPR detection is carried out by manual pipetting, which is laborious, time-consuming, and may increase the risk of contamination.[17] Also, they often require electronic equipment for heating and bulky instruments for detection, which significantly limits their capability at the point-of-care (POC).[18,19]

The combination of CRISPR-based molecular detection with microfluidics technology has pathed new ways for the next generation of POC diagnostics.[20,21] For example, centrifugal microfluidics integrated with a CRISPR-Cas13a assay was developed to detect food-borne pathogens.[22] A miniaturized microfluidic chip was developed to achieve automated micromixing for the CRISPR-Cas13a detection.[23] To reduce CRISPR fluorescence background signals, we pioneered an enclosed microfluidic chip patterned with high-aspect-ratio micropillars.[24] These microfluidic platforms, however, either require a time-consuming and labor-intensive fabrication process or rely on bulky electronic instruments for signal readout.

[a] Department of Mechanical Engineering, Kate Gleason Collage of Engineering, Rochester Institute of Technology, Rochester, NY 14623, United States
[b] Biological Mimetics, Inc. 124 Byte Drive, Frederick, MD 21702, United States
[c] Department of Electrical and Computer Engineering, University of Georgia, Athens, GA 30602, United States

In this study, we present a Funnel Adapted Sensing Tube (FAST) integrated with RPA amplification and CRISPR cleavage for power-free, pipette-free, and sensitive nucleic acid detection. The chip is designed with four chambers separated by carbon fiber rods to store RPA-CRISPR reagents. By simply pulling the rods, the reagents are mixed, leading to instrument-free detection. A low-cost hand warmer pouch (self-contained exothermal reaction) is used as a heating source for the entire reaction. With flashlight illumination, the fluorescence signal is detected by the naked eye in the dark. The fabrication process for FAST based on the water-soluble polymer is rapid, inexpensive, and environmentally friendly. The spike glycoprotein of SARS-CoV-2 plays a key role in host invasion[25,26]; therefore, the 703 bp DNA encoding the spike protein was selected as a target in this study, and our chip achieves a detection sensitivity of 10 fM (6 x 10^3 copies/μL). We also successfully develop a pipeline for automatic fluorescence reading with computer vision, providing a ~100% accuracy in FAST. Our simple, affordable, and sensitive molecular diagnostic platform will be a promising tool for POC diagnostics of COVID-19 and other emerging diseases in resource-limited settings without diagnostic errors or bias.

Experimental methods

a. Preparation of the SARS-CoV-2 target

DNA encoding S glycoprotein of Wuhan-Hu-1 isolate of SARS-CoV-2 (NC_045512.2, nucleotides 24708-25470) was synthesized by Genscript (Piscataway, NJ) and inserted into pUC57 to generate pUC57-SARS-CoV-2. The resulting constructs were transformed into DH5α *Escherichia coli*, propagated, and confirmed by DNA sequencing analysis (Poochon Scientific, Frederick, MD). An 879 bp fragment for SARS-CoV-2 target was excised from the plasmids using PvuII and NotI and gel purified using the GENECLEAN® Kit (MP-bio, Irvine, CA). The size and approximate concentration were verified using agarose gel electrophoresis. The final concentration was determined via UV absorbance spectroscopy (Beckman Coulter DU-530 UV-Vis Spectrophotometer).

b. Preparation of the influenza target

A 587 bp region of the Influenza A virus H3 gene (A/Wyoming/3/2003(H3)) was PCR amplified from plasmid p1041 (pTRIEX1.1 containing the full-length H3 gene). PCR was performed using Promega Go Taq master mix (Promega, Madison, WI) in a Denville express gene thermal cycler using F'-GCATCACTCCAAATGGAAGC and R'-GGCATTGTCACATTTGTGG, to give a 587 bp fragment. The fragment was purified using GENECLEAN® Kit (MP-bio, Irvine, CA). The size and approximate concentration were verified using agarose gel electrophoresis. The final concentration was determined via UV absorbance spectroscopy (Beckman Coulter DU-530 UV-Vis Spectrophotometer).

c. RPA amplification and CRISPR-Cas12a cleavage

TwistAmp® Basic kit was purchased from TwistDx™ Limited (Cambridge, UK). AsCas12a (Alt-R® A.s. Cas12a Ultra), SARS-CoV control, MERS-CoV control, and human RPP30 gene control (Hs_RPP30_PC) were all purchased from Integrated DNA Technologies (Coralville, IA). The RPA primers for the SARS-CoV-2 target were designed using NCBI-BLAST, based on the vendor's instructions. Synthetic oligonucleotides, including crRNA, primers, and fluorophore-quencher reporters were all synthesized by Integrated DNA Technologies and documented in **Supplement (Table 1)**. Binding buffer (NEBuffer™ r2.1) was purchased from New England Biolabs (Ipswich, MA).

We first mixed 6.32 μL of RPA primers (10 μM) and 3.68 μL of nuclease-free water. Then, the mixture was transferred to a microtube containing a TwistAmp® Basic reaction pellet. After dissolving the pellet, 38.8 μL of rehydration buffer and 11 μL of target were added to the mixture. The amplification process was activated by adding 14.42 mM of magnesium acetate and 6.58 μL of nuclease-free water. The reaction was incubated at 37 °C for 20 min. After incubation, the RPA amplicons were distributed into individual reaction tubes containing 15 μL of pre-assembled CRISPR-Cas12a complexes (5 μM of Cas12a (2 μL), 5 μM of crRNA (2 μL), 100 μM of ssDNA-FQ reporters (1 μL), and 3 μL of 1x Binding buffer). The mixture was incubated at 37 °C for 30 min.

d. Fabrication of FAST

To fabricate the FAST, the geometry of the reaction chambers was printed with water-soluble polyvinyl alcohol (PVA) resin as a molding core, using a Flashforge 3D printer (SainSmart). Then, the core was assembled into a customized aluminum mold. The silicone elastomeric base and curing agent (SYLGARDTM 184 Silicone Elastomer Kit) were mixed at a weight ratio of 10:1 and injected into the mold. Once filled with PDMS, the mold was degassed in a vacuum desiccator for 2 hrs to remove any trapped air bubbles before being baked at 65 °C for 12 hrs under atmospheric pressure. After curing, FAST was removed from the mold and immersed in deionized water with ultrasonic vibrations to dissolve the PVA core. Finally, the device was cut into two separate pieces, which are FAST A and B, and the 3.5-mm-diameter carbon fiber rods were inserted into the holes on the side of FAST A and B. Carbon fiber rods were chosen to separate each chamber because of the following advantages: 1) high chemical resistance, 2) low weight, 3) high temperature tolerance, 4) low thermal expansion, 5) high stiffness, and 6) no fluorescence when illuminated by a flashlight. The fabricated FAST A and B were sterilized and stored at room temperature in a UV Sterilizer Cabinet.

e. Reagent loading into FAST

A mixture of 6.32 μL of RPA primers, 3.68 μL of nuclease-free water, and a resuspended reaction pellet was introduced into the top first chamber of FAST A. Rehydration buffer (38.8 μL) was introduced into the second chamber of FAST A. A mixture of 3.42 μL of magnesium acetate and 6.58 μL of

nuclease-free water was filled into the third chamber of FAST A. The CRISPR-Cas12a complex was introduced into the FAST B.

f. SARS-CoV-2 fragment detection with FAST

To start the reaction, the second carbon rod in FAST A was pulled, allowing reagents from the first chamber to be transported to the second chamber with gravity. The ~11 µL of SARS-CoV-2 fragment at various concentrations was introduced into the second chamber with a syringe (Hamilton Company, Reno, NV) and a microtubing (Scientific Commodities, AZ). Next, the third rod was pulled, allowing reagents in the second and third chambers to mix. To avoid any aerosol contamination, FAST A was sealed with a PCR sealer tape (Bio-Rad, Hercules, CA). The chip was manually rotated up and down four times and wrapped in a hand warmer (HotHands Hand Warmers) for 20 min. After target amplification, FAST A was placed on top of FAST B. With the rod pulled, the amplicons were transferred from A to B. The chip was again sealed with a PCR sealer tape and wrapped in a hand warmer for 30 min. Following the reaction, the chip was illuminated by a handheld flashlight (emission: 470 nm) in the dark, and the image was recorded by a digital camera (exposure time: 1/30 s; ISO value: 500). The fluorescence intensity was validated by a custom-designed and calibrated fluorometer.[37] To ensure the reproducibility of the results, every experiment was conducted three times on separate days, and each sample was measured three times.

g. FAST chip reading with computer vision and machine learning algorithms

To build a machine learning model, we extracted histogram features from the images, which count the pixel number at each intensity.[27] We chose the green channel to distinguish between positive and negative samples as the fluorophore-quencher reporters emit at 520 nm. We also converted the color images to grayscale images so that the intensity histogram was extracted as features. The green channel histogram and grayscale intensity histogram were fused together as the image feature for classification. To test which algorithm is more accurate for the classification, multiple classification algorithms, including support-vector machine kernels (linear, polynomial, RBF, sigmoid), decision tree, KNN, and Naïve Bayesian algorithm, were performed and compared.[28,29,30,31,32,33]

Results

The fabrication process of the FAST chips is shown in **Fig. 1a** and consists of four main steps (printing, molding, dissolving, and assembly). First, the sacrificial core was printed with PVA. After that, the core was assembled into a customized aluminum mold, and the PDMS mixture was poured into the mold to create a PDMS replica. After dissolving the PVA core with water, the PDMS replica was cut into two separate pieces (FAST A and B). The pull-out carbon fiber rods, as gates, were assembled into FAST A and B to control the liquid flow and mix. FAST A has three chambers that are used for target amplification. FAST B has only one chamber which is used for visual detection. **Fig. 1b** shows a photograph of a fabricated FAST chip filled with food dye, which can clearly be observed by the naked eye. The chambers are separated by carbon fiber rods, serving as valves. The volumes of each chamber from top to bottom are 32.1 µL, 36.6 µL, 42 µL, and 66.3 µL, respectively. The chambers in FAST A are cubic structures, and the chamber in FAST B is designed with a pyramid-structured bottom to better collect reaction products for detection. The pyramid structure has a narrower bottom, thus making the liquid collection easier.

In this work, the detection assay includes an RPA assay for target amplification and a CRISPR-Cas12a assay for non-specific collateral cleavage. An 879 bp DNA fragment containing 703 bp of SARS-CoV-2 Spike gene was used as the target sequence. As depicted in **Fig. 1c**, the target was first amplified by RPA amplification. The reaction includes three proteins: recombinases to bind primers, single-stranded binding proteins to stabilize displaced DNA strands, and DNA polymerases to elongate primers in the presence of dNTPs. Two target-specific primers were designed to bind the target at different binding sites. After incubation, the targets were exponentially amplified. Following that, the amplicons were incubated with CRISPR-Cas12a complexes. The Cas12a-crRNA complex contains 143 nM of Cas12a, 143 nM of crRNA, 3 µL of 1x Binding buffer and 1.43 nM of fluorophore-quencher reporters (/56-FAM/TTATT/3IABkFQ/). With the presence of the target DNA, the activated Cas12a cleaves the reporters, thereby releasing the fluorophore with distinct fluorescence signals.

Fig. 1d shows the visual detection process of the self-contained FAST chip. Prior to the reaction, RPA-CRISPR reagents were loaded into the different chambers of the FAST. A mixture of primers and resuspended TwistAmp® Basic reaction pellet with a total volume of 10 µL was introduced into the top first chamber of FAST A. The rehydration buffer (38.8 µL) and a mixture of nuclease-free water and magnesium acetate (MgOAc) with a total volume of 10 µL were filled into the second and third chambers of FAST A, respectively. The CRISPR-Cas12a complex (15 µL) was introduced into FAST B. After the reagents loading into FAST, the chip was ready for viral detection. First, the amplification reaction was initiated by pulling carbon rods, allowing reagents to mix with the added DNA template. After incubation for 20 min, the amplicons were transferred from FAST A to B to initiate the CRISPR reaction. To facilitate power-free molecular detection, both RPA amplification and the CRISPR-Cas cleavage reaction were heated by a disposable hand warmer pouch. The fluorescence readouts were performed by illuminating FAST B with an inexpensive and portable flashlight.

To systematically evaluate our RPA-CRISPR assay, we prepared and tested eight reactions (#A-H) with various components. As shown in **Fig. 2a**, "+" indicates the presence of the component, whereas "-" indicates the absence of the component. The RPA-CRISPR reaction was initiated by incubating the RPA mix with 100 fM of the SARS-CoV-2 target at 37 ˚C for 20 min, followed by adding the remaining components

and incubating at 37 ˚C for 30 min. After the reaction, only #A, which contained RPA mix, crRNA, Cas12a, and the target, produced bright fluorescence signal, indicating successful target amplification and CRISPR cleavage. The signal of #A can easily be seen in the dark with a flashlight illumination (**Fig. 2b**). In contrast, for other reactions, no fluorescence signal was observed, indicating that missing any of the components would result in failed detection. To further validate the visual readouts, these reaction products were measured by a customized and calibrated fluorometer.[34] As expected, the normalized intensity of #A is higher than that of the other reactions (**Fig. 2c**).

Next, we evaluated the analytical sensitivity and specificity of the RPA-CRISPR assay for SARS-CoV-2 target detection. To determine the detection limit, we added different concentrations of SARS-CoV-2 samples into tubes containing the RPA mix. After incubation, the total amplicons were transferred into a microtube with 15 µL of the CRISPR-Cas complexes and incubated for 30 min. As presented in **Fig. 3a**, under flashlight illumination, an unambiguously distinct green fluorescence color is observed with a target concentration higher than 1 fM. In comparison, there are no obvious fluorescence signals in the reaction products without target input (#NC) or with target concentrations of 0.01 and 0.1 fM. These results were then validated using the customized fluorometer and are presented in **Fig. 3b**. The fluorescence intensities of the samples with a target concentration of 0.1, 1, 10, and 100 fM are significantly higher than the samples without the target input. The sensitivity is higher when measured with the fluorometer because the fluorometer provides stronger excitation than the flashlight, allowing more fluorophores to be excited. To evaluate the specificity of the RPA-CRISPR assay, we compared the fluorescence signal of SARS-CoV-2, Influenza, MERS-CoV, Human RPP30 Gene, and SARS-CoV fragment with a target concentration of 100 fM. As shown in **Fig. 3c**, only the SARS-CoV-2 target reaction product shows a distinct green color. The fluorescence intensities of these products were also measured with the fluorometer to validate the visual readouts (**Fig. 3d**). The fluorescence intensity of the SARS-CoV-2 sample is significantly higher than other samples, indicating that our RPA-CRISPR assay has excellent specificity.

We then evaluated FAST as a substitute for conventional microtubes in the RPA-CRISPR assay. First, the freshly prepared CRISPR-Cas12a complexes were mixed with 1 nM SARS-CoV-2 target and loaded into both Eppendorf microtubes and FAST B, which were then incubated on a hot plate simultaneously. The results presented in **Fig. 4a** indicate that the assay incubated in a microtube and FAST B generates comparable fluorescence signals. Next, RPA-CRISPR assays were prepared and loaded into microtubes or FAST chips for incubation. As shown in **Fig. 4b**, both assays with 100 fM target input generate high and comparable fluorescence signals (~0.8-1 counts) and are significantly higher than the assays without target input (~0.1 counts). After that, we evaluated the reaction performance with a hand warmer as a heating source. One CRISPR-Cas12 reaction was performed in microtube and heated by a hot plate, while another was performed in FAST B and heated by a hand warmer. As shown in **Fig. 4c**, the fluorescence signal produced in FAST B is comparable to the assay performed in a microtube. Next, low copies of the viral DNA target (100 fM) were amplified and detected in FAST by using a hand warmer as the heating source. **Fig. 4d** shows the comparable fluorescence signals of both the traditional RPA-CRISPR reaction heated by a hot plate and the FAST RPA-CRISPR reaction heated by a hand warmer.

With the established FAST chip and the RPA-CRISPR assay in hand, we then evaluated the sensitivity and specificity of the FAST for on-chip SARS-CoV-2 target detection. We added 11 µL of the target DNA into FAST containing the RPA and CRISPR complexes. The photographs presented in **Fig. 5a** show the color difference of each reaction product under the flashlight irradiation. A distinct fluorescence color is observed with the target concentration higher than 10 fM, which is consistent with the fluorescence signals measured by the fluorometer (**Fig. 5b**). In this work, the detection sensitivity is determined by visible readouts with a flashlight excitation, which is 10 fM. With a target concentration higher than 100 fM, the fluorescence intensity is saturated as almost all the FRET reporters were cleaved by the CRISPR complex. The specificity is determined by detecting 100 fM of SARS-CoV-2, Influenza, Human RPP30 Gene, MERS-CoV, and SARS-CoV target. As shown in **Fig. 5d**, under flashlight illumination, the reaction product with the SARS-CoV-2 input shows a strong green fluorescence color. The products with other target inputs, on the other hand, do not exhibit any strong fluorescence signals. These results were further confirmed by using the fluorometer and are presented in **Fig. 5d**. The intensity of matched SARS-COV-2 DNA is significantly higher than that of negative controls.

Fig. 6 shows the pipeline for the computer vision and machine learning based classification in FAST, which includes feature generation, intensity range selection, and feature classification. To train a robust model, we extracted and classified the features by using the images from both microtubes and FAST. As images of positive and negative control samples have distinct color and intensity distribution, we used this characteristic to extract features. Since black background takes up the large component of the image, pixels with zero intensity values compose the majority of the color intensity histogram, making it difficult to distinguish between the images. To address this issue, we selected a histogram range that allowed us to clearly distinguish between the histogram features of positive and negative samples. Instead of counting the entire intensity range, we only chose intensity from 100 to 255 for color image histogram and 50 to 255 for grayscale intensity image histogram, allowing positive and negative samples to be distinguished. With these more perceptible features, we trained the classifiers to classify the images. Linear Kernel performs best, with classification accuracy closing to 100%, mainly owing to the easy separation of the features.

Discussion

We developed a simple, portable, and easy-to-use microfluidic chip for on-site nucleic acids detection. Coupled with RPA amplification and CRISPR-Cas12a detection assay, the FAST chip can detect nucleic acids in a sensitive, rapid (<1 hr), and isothermal manner. Compared to benchtop-based molecular diagnostics such as RT-PCR, our FAST chip is simpler in the following aspects: 1) operation – the viral detection is completed by manually pulling off the carbon roads, which removes time-consuming and error-prone pipetting; 2) incubation condition – the detection process is electrical-free, with a portable and inexpensive hand warmer pouch serving as the heating source; 3) measurement – Unlike conventional bioassays that require bulky sensing instruments, our detection strategy provides visible readouts with portable flashlight illumination.[35,36,34,37] All of these advantages demonstrate that our FAST chip is a simple, portable, and easy-to-use detection system, designed for POC applications.

In addition, FAST is an excellent substitute to commercial microtubes. The molecular reactions within FAST are stable and unaffected by the compositions of the chip. As shown in Fig. 4, the reactions in FAST are comparable to those in microtubes. No significant protein adsorption in the chip is observed, and the detection sensitivity is comparable to those obtained in microtubes with manual pipetting. As a self-contained platform, PDMS-made chambers are perfectly sealed by the carbon rods, with no reagent leaking observed. Amplification and detection are combined in the enclosed FAST chip, significantly reducing the risk of contamination during amplicon transfer. The unique design of FAST makes its operation simple enough for individuals without training. In comparison to established lateral flow strips, our chip allows the pre-loading of the reagents, eliminating the need for pipetting during sample preparation.[38,39] In the future, the number and volume of chambers can be modified to accommodate different types of bioassays.[40,41]

Another unique advantage of FAST chip is its simple and inexpensive fabrication process. The 3D printed water-soluble core is used as a sacrificial template to replicate the complex chamber design of FAST in PDMS with high precision. In comparison to many other published platforms, FAST does not require a cleanroom setting or expensive instruments for fabrication.[42,43] The entire fabrication can be completed in a single day, and multiple chips can be fabricated simultaneously, laying the basis for massive detection. The 3D printer utilized in this work costs less than $1,000, which is affordable for most small labs and startups. For mass production, water-soluble cores can be manufactured by injection molding to further improve the production rate.

With only flashlight illumination and visual observation, our FAST chip can detect the SARS-CoV-2 target with a sensitivity of 10 fM (6 x 10^3 copies/μL). To further improve the sensitivity, our RPA-CRISPR reaction can be improved by adding additive and divalent-metal-ion or combining with multiple crRNA.[44,45,46] Our FAST chip also exhibits excellent specificity as it can distinguish the SARS-CoV-2 target from negative controls with genome similarity (SARS-CoV, MERS-CoV, and Influenza).[47,48]

As a fully transparent device, FAST can be illuminated by a portable flashlight and imaged by a smartphone or a digital camera.[49,50] We realized automatic sample quantification by using a Kernel classifier. There are several advantages of using computer vision for viral detection: 1) this machine learning algorithm improves the reliability and accuracy of naked-eye based detection, especially important for low-concentration samples; 2) with more data collected in FAST, a deep learning model can be built with a 100% accuracy, thus eliminating the need to build an internal control in FAST; 3) a simple mobile app can be designed based on our Linear Kernel to enable a sample-in and answer-out system without adding other hardware components.[51,52,53]

Currently, the reagents are pre-loaded into the chip prior to the reaction. Considering the difficulty of achieving cold-chain transportation and storage in remote settings, the RPA and CRISPR reagents can be lyophilized into the chambers and stored at room temperature for an extended period of time.[54,55] FAST chip shows minimal non-specific binding, but additional modifications such as chemical surface coating can be applied to further minimize molecular binding during long-term storage.[56,57] To further facilitate on-site diagnostics, target extraction and reverse transcription modules can be integrated into the FAST to create a fully integrated "sample-to-result" viral detection platform. By adding a well-established reverse transcription process, our chip can easily be adapted to work with RNA-based viruses.[58,59] In this work, the performance of FAST was evaluated at room temperature. Future tests need be conducted to ensure FAST's compatibility with varying climatic conditions.

In this work, we demonstrate the feasibility of the computer vision-enabled automatic detection of SARS-CoV-2 fragment by using only one single set of chambers loaded with primers and crRNA specific to the SARS-CoV-2 target. To enable multi-target detection, our chip can be easily modified with a split valve and an additional set of chambers. Each set of the chambers can be loaded with RPA-CRISPR reagents that are specific to certain nucleic acid targets. After loading the patient sample, the split valve can divide the sample into equal volumes that are distributed to two columns of chambers for dual-detection of different nucleic acid targets.

Author Contributions

M. Bao and S. Zhang contributed equally to this work. M. Bao, R. Liu, G. Lu, G. Tobin, and K. Du designed the experiments. M. Bao, S. Zhang, C. ten Pas, and F. Yuqing conducted the experiments. S. Dollery and R. Bushnell prepared the viral samples. M. Bao, S. Zhang, and K. Du wrote the manuscript. All authors commented the manuscript.

Conflicts of interest

There are no conflicts to declare.

Acknowledgments

The authors would like to thank Yuchen Zhong and Mary Nguyen at RIT for the schematic design.

References

1 WHO Coronavirus (COVID-19) Dashboard, https://covid19.who.int).
2 S. Perlman, *New England Journal of Medicine*, 2020, **382**, 760-762.
3 G. Huang, T. Gong, G. Wang, J. Wang, X. Guo, E. Cai, S. Li, X. Li, Y. Yu and L. Lin, *American Journal of Roentgenology*, 2020, **215**, 367-373.
4 M. Johnson, H. R. Wagstaffe, K. C. Gilmour, A. L. Mai, J. Lewis, A. Hunt, J. Sirr, C. Bengt, L. Grandjean and D. Goldblatt, *Journal of Clinical Virology*, 2020, **130**, 104572.
5 G. M. Bwire, M. V. Majigo, B. J. Njiro and A. Mawazo, *Journal of Medical Virology*, 2020, DOI: 10.1002/jmv.26349, 10.1002/jmv.26349.
6 S. Petralia and S. Conoci, *ACS Sens.*, 2017, **2**, 876-891.
7 S. Suleman, S. K. Shukla, N. Malhotra, S. D. Bukkitgar, N. P. Shetti, R. Pilloton, J. Narang, Y. Nee Tan and T. M. Aminabhavi, *Chemical Engineering Journal*, 2021, **414**, 128759.
8 M. M. Kaminski, O. O. Abudayyeh, J. S. Gootenberg, F. Zhang and J. J. Collins, *Nat Biomed Eng*, 2021, **5**, 643-656.
9 W. Feng, A. M. Newbigging, J. Tao, Y. Cao, H. Peng, C. Le, J. Wu, B. Pang, J. Li, D. Lorne Tyrrell, H. Zhang and X. Chris Le, *Chemical Science*, 2021, **12**, 4683-4698.
10 J. S. Chen, E. Ma, L. B. Harrington, M. D. Costa, X. Tian, J. M. Palefsky and J. A. Doudna, *Science*, 2018, **360**, 436-439.
11 M. J. Kellner, J. G. Koob, J. S. Gootenberg, O. O. Abudayyeh and F. Zhang, *Nature Protocols*, 2019, **14**, 2986-3012.
12 H. Rahimi, M. Salehiabar, M. Barsbay, M. Ghaffarlou, T. Kavetskyy, A. Sharafi, S. Davaran, S. C. Chauhan, H. Danafar, S. Kaboli, H. Nosrati, M. M. Yallapu and J. Conde, *ACS Sens.*, 2021, **6**, 1430-1445.
13 L. Zhou, R. Peng, R. Zhang and J. Li, *Journal of Cellular and Molecular Medicine*, 2018, **22**, 5807-5815.
14 L. Zhang, F. Tian, C. Liu, Q. Feng, T. Ma, Z. Zhao, T. Li, X. Jiang and J. Sun, *Lab Chip*, 2018, **18**, 610-619.
15 F. Tian, C. Liu, J. Deng, Z. Han, L. Zhang, Q. Chen and J. Sun, *Sci. China Chem.*, 2020, **63**, 1498-1506.
16 W. Feng, H. Peng, J. Xu, Y. Liu, K. Pabbaraju, G. Tipples, M. A. Joyce, H. A. Saffran, D. L. Tyrrell, S. Babiuk, H. Zhang and X. C. Le, *Anal. Chem.*, 2021, **93**, 12808-12816.
17 F. Li, J. Xiao, H. Yang, Y. Yao, J. Li, H. Zheng, Q. Guo, X. Wang, Y. Chen, Y. Guo, Y. Wang and C. Shen, *Front. Microbiol.*, 2022, **13**, 858806.
18 H. Liu, J. Wang, H. Zeng, X. Liu, W. Jiang, Y. Wang, W. Ouyang and X. Tang, *Food Chemistry*, 2021, **334**, 127608.
19 M. H. Choi, J. Lee and Y. J. Seo, *Analytica Chimica Acta*, 2021, **1158**, 338390.
20 A. Ramachandran, D. A. Huyke, E. Sharma, M. K. Sahoo, C. Huang, N. Banaei, B. A. Pinsky and J. G. Santiago, *PNAS*, 2020, **117**, 29518-29525.
21 N. L. Welch, M. Zhu, C. Hua, J. Weller, M. E. Mirhashemi, T. G. Nguyen, S. Mantena, M. R. Bauer, B. M. Shaw, C. M. Ackerman, S. G. Thakku, M. W. Tse, J. Kehe, M.-M. Uwera, J. S. Eversley, D. A. Bielwaski, G. McGrath, J. Braidt, J. Johnson, F. Cerrato, G. K. Moreno, L. A. Krasilnikova, B. A. Petros, G. L. Gionet, E. King, R. C. Huard, S. K. Jalbert, M. L. Cleary, N. A. Fitzgerald, S. B. Gabriel, G. R. Gallagher, S. C. Smole, L. C. Madoff, C. M. Brown, M. W. Keller, M. M. Wilson, M. K. Kirby, J. R. Barnes, D. J. Park, K. J. Siddle, C. T. Happi, D. T. Hung, M. Springer, B. L. MacInnis, J. E. Lemieux, E. Rosenberg, J. A. Branda, P. C. Blainey, P. C. Sabeti and C. Myhrvold, *Nature Medicine*, 2022, **28**, 1083-1094.
22 C. R. Phaneuf, K. J. Seamon, T. P. Eckles, A. Sinha, J. S. Schoeniger, B. Harmon, R. J. Meagher, V. V. Abhyankar and C.-Y. Koh, *Analytical Methods*, 2019, **11**, 559-565.
23 P. Qin, M. Park, K. J. Alfson, M. Tamhankar, R. Carrion, J. L. Patterson, A. Griffiths, Q. He, A. Yildiz, R. Mathies and K. Du, *ACS Sens.*, 2019, **4**, 1048-1054.
24 K. N. Hass, M. Bao, Q. He, L. Liu, J. He, M. Park, P. Qin and K. Du, *ACS Omega*, 2020, **5**, 27433-27441.
25 Y. Huang, C. Yang, X.-f. Xu, W. Xu and S.-w. Liu, *Acta Pharmacol Sin*, 2020, **41**, 1141-1149.
26 E. Ortiz-Prado, K. Simbaña-Rivera, L. Gómez- Barreno, M. Rubio-Neira, L. P. Guaman, N. C. Kyriakidis, C. Muslin, A. M. G. Jaramillo, C. Barba-Ostria, D. Cevallos-Robalino, H. Sanches-SanMiguel, L. Unigarro, R. Zalakeviciute, N. Gadian and A. López-Cortés, *Diagnostic Microbiology and Infectious Disease*, 2020, **98**, 115094.
27 V. K. Chauhan, K. Dahiya and A. Sharma, *Artif Intell Rev*, 2019, **52**, 803-855.
28 D.-X. Zhou and K. Jetter, *Adv Comput Math*, 2006, **25**, 323-344.
29 B.-C. Kuo, H.-H. Ho, C.-H. Li, C.-C. Hung and J.-S. Taur, *IEEE Journal of Selected Topics in Applied Earth Observations and Remote Sensing*, 2014, **7**, 317-326.
30 J. Jebadurai and J. D. Peter, *Pattern Recognition Letters*, 2017, **94**, 144-153.
31 Y.-y. Song and Y. Lu, *Shanghai Arch Psychiatry*, 2015, **27**, 130-135.
32 L. Jiang, Z. Cai, D. Wang and S. Jiang, Fourth International Conference on Fuzzy Systems and Knowledge Discovery (FSKD 2007), 2007.
33 Encyclopedia of Bioinformatics and Computational Biology: ABC of Bioinformatics, Elsevier, 2018.
34 Q. He, D. Yu, M. Bao, G. Korensky, J. Chen, M. Shin, J. Kim, M. Park, P. Qin and K. Du, *Biosensors and Bioelectronics*, 2020, **154**, 112068.
35 H. G. Barreto, F. A. de Pádua Milagres, G. C. de Araújo, M. M. Daúde and V. A. Benedito, *J Mol Med (Berl)*, 2020, **98**, 1727-1736.
36 M. Bao, E. Jensen, Y. Chang, G. Korensky and K. Du, *ACS Appl. Mater. Interfaces*, 2020, **12**, 43435-43443.
37 Y. Tao, K. Yi, H. Wang, K. Li and M. Li, *Sensors and Actuators B: Chemical*, 2022, **361**, 131711.
38 J. Qian, D. Huang, D. Ni, J. Zhao, Z. Shi, M. Fang and Z. Xu, *Food Control*, 2022, **132**, 108485.
39 N. Wei, B. Zheng, J. Niu, T. Chen, J. Ye, Y. Si and S. Cao, *Viruses*, 2022, **14**, 179.
40 X. Cheng, Y. Yan, X. Chen, J. Duan, D. Zhang, T. Yang, X. Gou, M. Zhao, S. Ding and W. Cheng, *Sensors and Actuators B: Chemical*, 2021, **331**, 129458.
41 A. E. Calvert, B. J. Biggerstaff, N. A. Tanner, M. Lauterbach and R. S. Lanciotti, *PLOS ONE*, 2017, **12**, e0185340.
42 Z. Qi, L. Xu, Y. Xu, J. Zhong, A. Abedini, X. Cheng and D. Sinton, *Lab Chip*, 2018, **18**, 3872-3880.

43 N. C. Speller, G. G. Morbioli, M. E. Cato, T. P. Cantrell, E. M. Leydon, B. E. Schmidt and A. M. Stockton, *Sensors and Actuators B: Chemical*, 2019, **291**, 250-256.
44 M. Lin, H. Yue, T. Tian, E. Xiong, D. Zhu, Y. Jiang and X. Zhou, *Anal. Chem.*, 2022, **94**, 8277-8284.
45 P. Ma, Q. Meng, B. Sun, B. Zhao, L. Dang, M. Zhong, S. Liu, H. Xu, H. Mei, J. Liu, T. Chi, G. Yang, M. Liu, X. Huang and X. Wang, *Adv Sci (Weinh)*, 2020, **7**, 2001300.
46 P. Fozouni, S. Son, M. Díaz de León Derby, G. J. Knott, C. N. Gray, M. V. D'Ambrosio, C. Zhao, N. A. Switz, G. R. Kumar, S. I. Stephens, D. Boehm, C.-L. Tsou, J. Shu, A. Bhuiya, M. Armstrong, A. R. Harris, P.-Y. Chen, J. M. Osterloh, A. Meyer-Franke, B. Joehnk, K. Walcott, A. Sil, C. Langelier, K. S. Pollard, E. D. Crawford, A. S. Puschnik, M. Phelps, A. Kistler, J. L. DeRisi, J. A. Doudna, D. A. Fletcher and M. Ott, *Cell*, 2021, **184**, 323-333.e329.
47 X. Tang, C. Wu, X. Li, Y. Song, X. Yao, X. Wu, Y. Duan, H. Zhang, Y. Wang, Z. Qian, J. Cui and J. Lu, *National Science Review*, 2020, **7**, 1012-1023.
48 Z. Wu, D. Harrich, Z. Li, D. Hu and D. Li, *Rev Med Virol*, 2020, DOI: 10.1002/rmv.2171, e2171.
49 K. Trofymchuk, V. Glembockyte, L. Grabenhorst, F. Steiner, C. Vietz, C. Close, M. Pfeiffer, L. Richter, M. L. Schütte, F. Selbach, R. Yaadav, J. Zähringer, Q. Wei, A. Ozcan, B. Lalkens, G. P. Acuna and P. Tinnefeld, *Nat Commun*, 2021, **12**, 950.
50 B. Ning, T. Yu, S. Zhang, Z. Huang, D. Tian, Z. Lin, A. Niu, N. Golden, K. Hensley, B. Threeton, C. J. Lyon, X.-M. Yin, C. J. Roy, N. S. Saba, J. Rappaport, Q. Wei and T. Y. Hu, *Science Advances*, 2020, DOI: 10.1126/sciadv.abe3703, eabe3703.
51 F. Cui, Y. Yue, Y. Zhang, Z. Zhang and H. S. Zhou, *ACS Sens.*, 2020, **5**, 3346-3364.
52 M. A. Mujawar, H. Gohel, S. K. Bhardwaj, S. Srinivasan, N. Hickman and A. Kaushik, *Materials Today Chemistry*, 2020, **17**, 100306.
53 D. Quesada-González and A. Merkoçi, *Biosensors and Bioelectronics*, 2017, **92**, 549-562.
54 F. Stumpf, F. Schwemmer, T. Hutzenlaub, D. Baumann, O. Strohmeier, G. Dingemanns, G. Simons, C. Sager, L. Plobner, F. v. Stetten, R. Zengerle and D. Mark, *Lab Chip*, 2016, **16**, 199-207.
55 Z. Li, X. Ding, K. Yin, L. Avery, E. Ballesteros and C. Liu, *Biosens Bioelectron*, 2022, **199**, 113865.
56 K. M. Kovach, J. R. Capadona, A. S. Gupta and J. A. Potkay, *Journal of Biomedical Materials Research Part A*, 2014, **102**, 4195-4205.
57 A. Gökaltun, Y. B. Kang, M. L. Yarmush, O. B. Usta and A. Asatekin, *Sci Rep*, 2019, **9**, 7377.
58 D. Xiong, W. Dai, J. Gong, G. Li, N. Liu, W. Wu, J. Pan, C. Chen, Y. Jiao, H. Deng, J. Ye, X. Zhang, H. Huang, Q. Li, L. Xue, X. Zhang and G. Tang, *PLOS Biology*, 2020, **18**, e3000978.
59 Y. Sun, L. Yu, C. Liu, S. Ye, W. Chen, D. Li and W. Huang, *Journal of Translational Medicine*, 2021, **19**, 74.

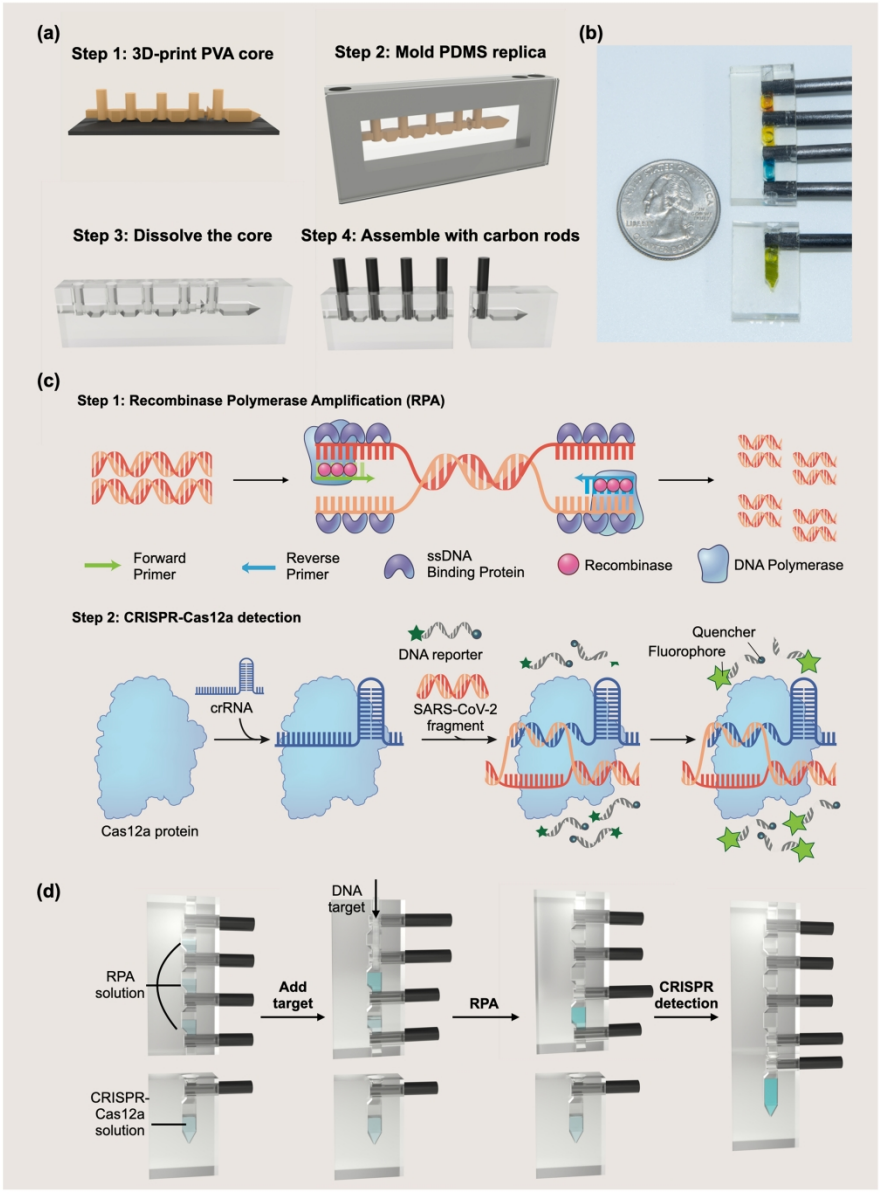

Figure 1. (a) Scheme for the FAST chip fabrication. (b) Photograph of FAST filled with food dye. (c) Principle of SARS-CoV-2 fragment detection using RPA amplification and CRISPR cleavage. (d) Working principle of the FAST for visual detection of SARS-CoV-2 fragment.

1312x1765mm (72 x 72 DPI)

(a)

	A	B	C	D	E	F	G	H
RPA mix	+	+	-	+	+	-	+	+
crRNA	+	+	+	+	-	+	-	+
Cas12a	+	+	+	-	+	+	+	-
F-Q	+	+	+	+	+	+	+	+
SARS-CoV-2 fragment	+	-	-	-	-	+	+	+

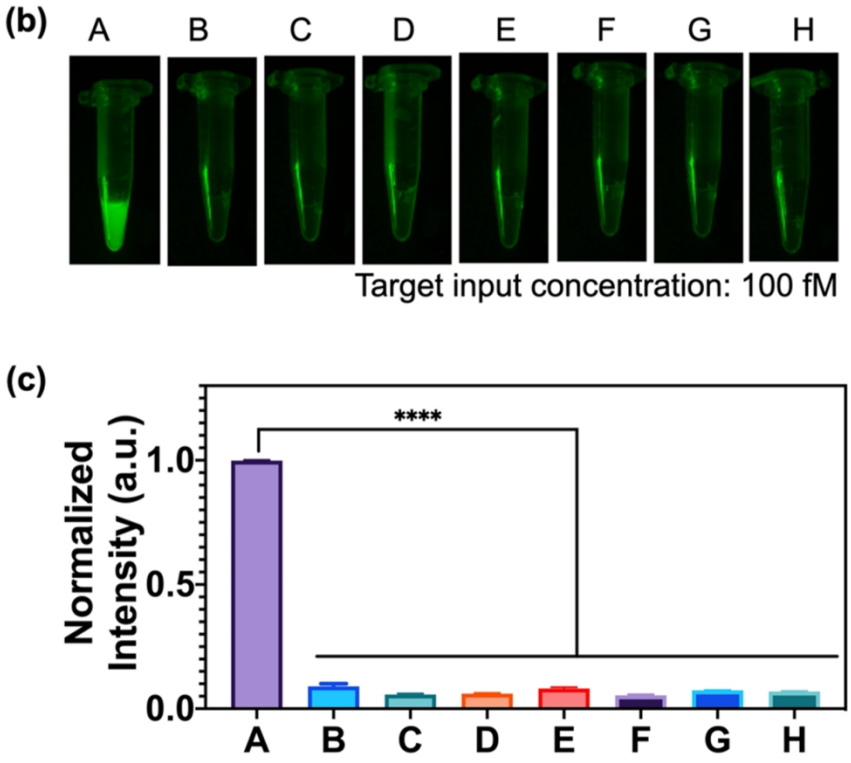

Figure 2. Evaluation of the RPA-CRISPR assay. (a) Eight evaluation reactions with various components. Reaction #A contains all of the components for RPA-CRISPR assay, whereas other reactions lack certain components. (b) Endpoint images of the reactions illuminated by a flashlight (wavelength: 470 nm). (c) Normalized fluorescence signals of the endpoint reactions. Statistical analyses were performed using unpaired t-test analysis (ns = $p > 0.05$; * = $0.01 < P \leq 0.05$; ** = $0.05 < P \leq 0.05$; *** = $0.01 < P \leq 0.001$; **** = $P \leq 0.0001$).

609x850mm (72 x 72 DPI)

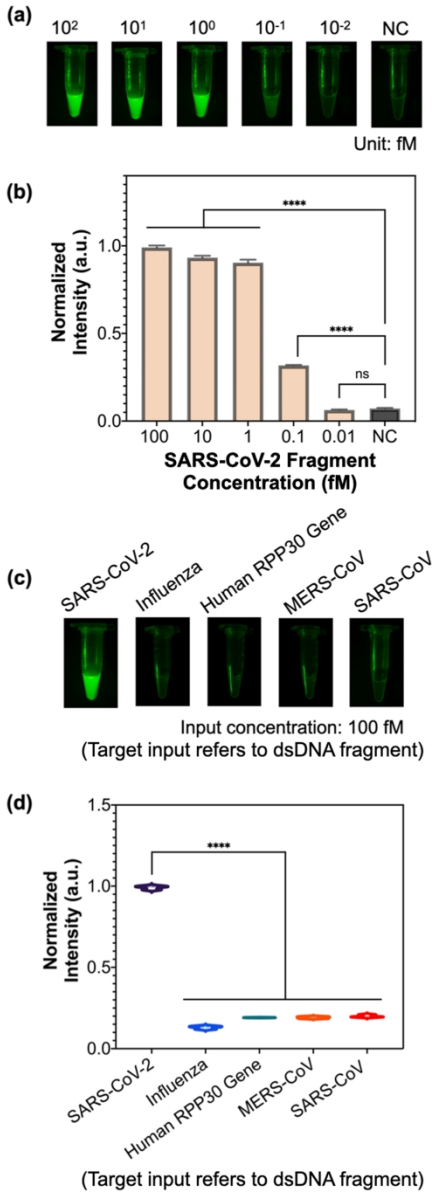

Figure 3. Evaluation of the RPA-CRISPR assay for SARS-CoV-2 target detection (performed in microtubes). (a) Endpoint fluorescence images of reaction with SARS-CoV-2 target and without target (NC) under a 470 nm flashlight. (b) Normalized fluorescence signals of the reaction products with and without SARS-CoV-2 target. (c) Endpoint fluorescence images of reaction with 100 fM of SARS-CoV-2, Influenza, Human RPP30 gene, MERS-CoV, and SARS-CoV target. The samples were illumined using a 470 nm flashlight. (d) Normalized fluorescence signals of the reactions with 100 fM of SARS-CoV-2 (purple), Influenza (blue), human RPP30 gene (green), MERS-CoV (orange), and SARS-CoV (red). Statistical analyses were performed using unpaired t-test analysis (ns = $p > 0.05$; * = $0.01 < P \leq 0.05$; ** = $0.05 < P \leq 0.05$; *** = $0.01 < P \leq 0.001$; **** = $P \leq 0.0001$).

469x1289mm (72 x 72 DPI)

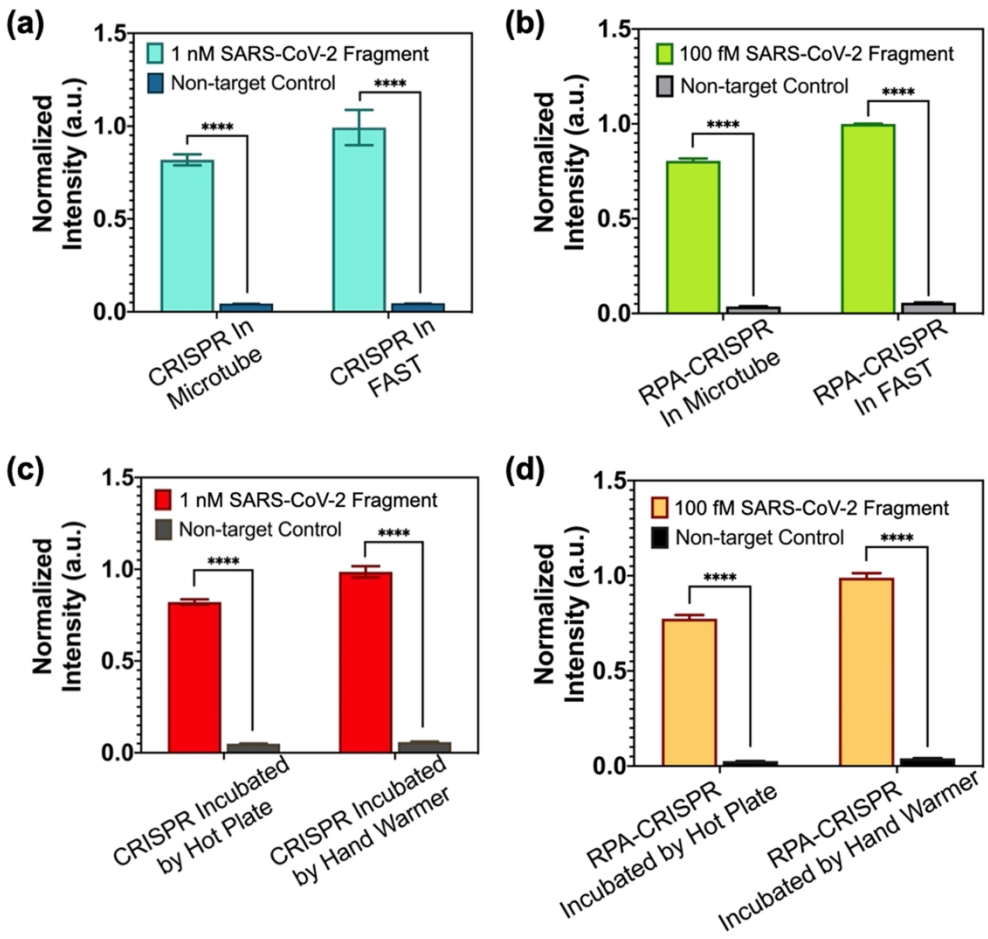

Figure 4. (a) CRISPR reaction incubated inside microtube versus FAST chip. The 1 nM of SARS-CoV-2 target was introduced into the CRISPR reaction solution. (b) RPA-CRISPR reaction incubated in microtube versus FAST chip. The 100 fM of SARS-CoV-2 target was added into the RPA reaction solution. After 20 min incubation, all amplicons were transferred into the CRISPR solution. (c) CRISPR reaction containing 1 nM SARS-CoV-2 fragment incubated by hot plate versus hand warmer. (d) RPA-CRISPR reaction containing 100 fM incubated with hot plate versus hand warmer. The reaction heated by hot plate was performed in microtubes, while the reaction heated by hand warmer was conducted in FAST chip. Statistical analyses were performed using unpaired t-test analysis (ns = $p > 0.05$; * = $0.01 < P \leq 0.05$; ** = $0.05 < P \leq 0.05$; *** = $0.01 < P \leq 0.001$; **** = $P \leq 0.0001$).

774x732mm (72 x 72 DPI)

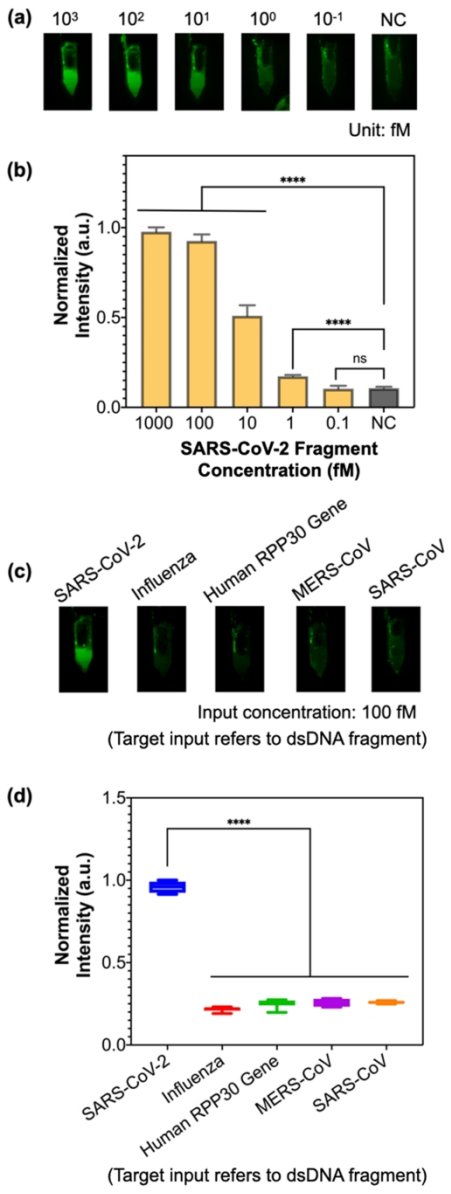

Figure 5. Performance evaluation of FAST chip for SARS-CoV-2 fragment detection. (a) Endpoint fluorescence images of reaction with and without SARS-CoV-2 target input. The reaction products were illuminated with a 470 nm flashlight. (b) Normalized fluorescence signal of the reaction products with input of SARS-CoV-2 target and no target. (c) Fluorescence images of the reaction products with the input of SARS-CoV-2, Influenza, MERS-CoV, Human RPP30 gene, and SARS-CoV (input concentration: 100 fM). (d) Normalized fluorescence signal of the reaction products with SARS-CoV-2 (blue), Influenza (red), human RPP30 gene (green), MERS-CoV (purple), and SARS-CoV (orange) as inputs. The concentration of target sequence is 100 fM. Statistical analyses were conducted using unpaired t-test analysis (ns = $p > 0.05$; * = $0.01 < P \leq 0.05$; ** = $0.05 < P \leq 0.05$; *** = $0.01 < P \leq 0.001$; **** = $P \leq 0.0001$).

383x1016mm (72 x 72 DPI)

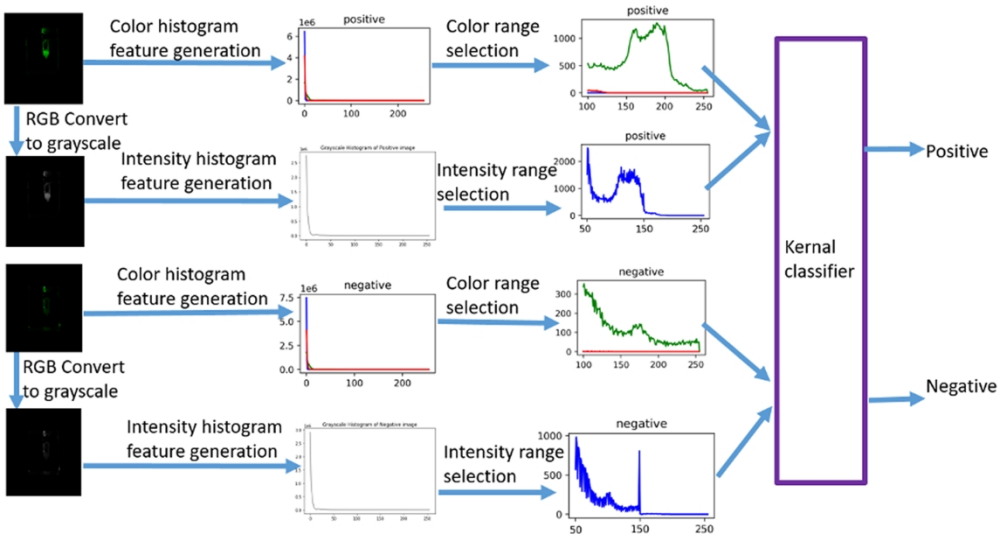

Figure 6. The pipeline for automatic positive and negative image classification, which involves histogram, feature generation, intensity range selection, and feature classification.

1375x740mm (72 x 72 DPI)